Photocatalytic degradation of contaminants of emerging concern using a low-cost and efficient black bismuth titanate-based water treatment reactor.

Matthieu Grao[a], James Redfern[b], Peter Kelly[a], Marina Ratova[a*],

[a] Advanced Materials and Surface Engineering Research Centre, Department of Engineering, Manchester Metropolitan University, Manchester M1 5GD, UK
[b] Department of Natural Sciences, Manchester Metropolitan University, Manchester, M1 5GD, UK

[*] Corresponding author: M. Ratova, Advanced Materials and Surface Engineering Research Centre, Manchester Metropolitan University, John Dalton Building, Chester Street, Manchester M1 5GD, UK, tel. +44 161 247 4648, e-mail address marina_ratova@hotmail.com; m.ratova@mmu.ac.uk

Abstract

Photocatalysis is recognized as a sustainable technology for wastewater treatment, but it is limited by its scalability and efficiency. Here, we report the fabrication of a bespoke photocatalytic reactor, made from readily available consumer market components. The reactor was loaded with glass rods coated with a bismuth titanate photocatalyst deposited by reactive pulsed DC magnetron sputtering. Bismuth titanate is a remarkable material, which has shown the property of increasing its photocatalytic capabilities over repeated usage due to photoinduced oxygen vacancies, forming oxygen-vacancy rich "black" bismuth titanate. The reactor was tested with different rod configurations and photocatalytic material was cycled over 25 times, equivalent to 125 h of consecutive use, against methylene blue dye under UV light. Orange II dye degradation tests carried out in the presence of scavengers revealed that photocatalytic reactions were driven by superoxide ($O_2^{\cdot -}$) and holes (h^+), when using pristine bismuth titanate and by superoxide ($O_2^{\cdot -}$), electrons (e^-) and holes (h^+), when using "black" bismuth titanate. Finally, the reactor was used to successfully degrade levofloxacin, a typical antibiotic, which was verified by UV-Vis (ultraviolet-visible) spectroscopy and inhibition zone tests in the presence of three different pathogens (*E. coli*, *S. aureus* and *A. baumannii*).

Keywords: Photocatalytic reactor; magnetron sputtering; wastewater treatment; bismuth titanate; antibiotics.

1. Introduction

High throughput manufacturing has improved the standards of living of the general population, but this comes at a cost. The presence of pollutants in water from industries, such as coal, dairy, textile, cannery, tannery, and paper, can be traced back to the 20th century [1]. More recently, pharmaceuticals, cosmetics, petrochemicals, pesticides, microplastics, dyes, heavy metals and others have become the major effluents all over the world and are sources of environmental and human hazards. According to the World Health Organization (WHO), more than two billion people still lack access to safely-managed water worldwide [2]. It is predicted that by 2025, half of the world's population will live in water-stressed areas [2]. As a result, access to adequate provision of water resources is considered a global priority and is named as one of the UN Sustainable Development Goals. This pressing issue calls for novel and sustainable technologies to be developed and implemented, until new global and environmentally sensible policies are adopted. Among the many pollutants found in wastewater, antibiotics are of particular concern.

Antibiotic resistance is the capacity for microorganisms (e.g. bacteria) to survive the usually damaging or lethal effects of antibiotic compounds. Whilst antibiotic resistance has always developed naturally, anthropogenic activities, especially the overuse of antibiotics, has resulted in a significant increase in the appearance of resistant microorganisms capable of causing deadly infections across the world. As such, the WHO has declared antimicrobial resistance one of the top ten global public health threats facing humanity [3]. Traces of antibiotics will inevitably make their way into the wastewater system as a result of human and animal excretion, due to incomplete metabolism, and disposal of unused drug wastes from pharmaceutical manufacturing processes [4]. In addition to this, wastewater provides an ideal location for bacterial growth due to the abundance of organic matter, the presence of oxygen and nitrate, stable temperatures and adequate pH [4]. These conditions, in addition to sub-inhibitory traces of antibiotics, can result in, and even increase rates relating to the evolution and transfer of resistance in and between bacteria [5,6], which can result in large numbers of antibiotic-resistant bacteria being discharged into other water systems. As such, removing antibiotics from wastewater is of critical importance.

Although there is a wide variety of wastewater treatment plants, they typically operate with the same sequential steps. First, wastewater undergoes a pre-treatment phase, where solid bulky wastes are removed and flowed into a primary sedimentation tank. Floating fats and sediments are removed and treated in sludge treatment facilities, while the remaining effluent is channelled into a secondary sedimentation tank [7]. The organic load in the wastewater is then considerably reduced through the use of biological process, such as activated sludges. The final tertiary step focuses on the inactivation of microorganisms and decomposition of pharmaceuticals, personal care products, pesticides etc. It is usually achieved through chlorination, UV (ultraviolet) radiation and ozonation [7]. Unfortunately, not only are those additional steps expensive, but they are not always sufficient. Thus, antibiotics in concentrations ranging from $\mu g.L^{-1}$ to $ng.L^{-1}$ were detected in wastewater treatment plant effluents in developed countries, such as Japan [8], United Kingdom [9], Sweden [10], Croatia [11], Spain [12], China [13], Slovakia [14], Germany and many more [15].

Photocatalysis is an advanced oxidation process (AOP) that was discovered in 1969 by Fujishima and Honda when studying the splitting of water by TiO_2 (titanium dioxide) under UV light [16]. When a photocatalyst semiconductor is irradiated by a light with of sufficient energy ($h\nu > E_g$), electron and hole pairs are formed in the conduction and valence band, respectively. These charge carriers diffuse to the surface and react with surrounding molecules to form radical species. To date photocatalysis has found many practical applications such as solar energy

[17,18], hydrogen production [19,20], self-cleaning surfaces [21], and self-sterilising coatings [22]. Among them, photocatalysis found a promising place in wastewater treatment, as it only requires a photocatalyst, light and water to decompose a wide range of pollutants, such as dyes [23–25], pharmaceuticals [26,27], microorganisms [28–30], pesticides [31,32] etc. To date, titanium dioxide is still the most widely studied and used photocatalyst, even though it suffers from rapid electron-hole recombination and can only utilise UV light, which accounts for less than 5% of the solar spectrum [33]. These two issues hinder the widespread adoption of photocatalytic wastewater treatment systems based on TiO_2. To address these issues, efforts have been undertaken to either modify TiO_2 [34–37], or use alternative photocatalysts [38–40]. In recent years, bismuth oxide-based photocatalysts have captured the attention of researchers, as possible alternatives to TiO_2. Bismuth oxide [29,30,41], vanadate [42], tungstate [43] and titanate [44] consistently displayed high photocatalytic activity and lower band gaps, compared to conventionally used titania. This work focuses on bismuth titanate (BT), which possesses two known photocatalytic polymorphs namely, $Bi_{12}TiO_{20}$ and $Bi_4Ti_3O_{12}$ [45,46]. The former belongs to the Sillenite family and is formed by a network of Bi–O polyhedra connected to TiO_4 tetrahedra [47]. The latter belongs to the Aurivillius family and composed of pseudo-perovskite units $(Bi_2Ti_3O_{10})^{2-}$, sandwiched by fluorite-like $(Bi_2O_2)^{2+}$ layers [48]. Like titanium dioxide, all bismuth titanate polymorphs are indirect bandgap materials [49]. Kallawar et al. reported that the bandgap values for the $Bi_{12}TiO_{20}$ polymorph range from 2.36 to 2.78 eV, which makes it a suitable candidate for visible-light photocatalysis [50]. In a previous study, a bismuth titanate composite, produced by magnetron sputtering, outperformed TiO_2 for both dye degradation and *E. coli* inactivation tests under UV-A [51]. Bismuth titanate was as much as 15 times more efficient at degrading MB under UV than anatase TiO_2 [51]. Furthermore, upon prolonged use bismuth titanate coatings have shown the remarkable property of producing photoinduced oxygen vacancies, which directly translated to a 6-fold increase in performance after 15 consecutive cycling tests. These oxygen vacancies appear to be responsible for the coating colour change from white to black and are believed to act as trapping sites for electrons, which increases their lifetime.

Induced defects in semiconductors is a strategy that has been extensively used in recent years, in particular with TiO_2, the most widely-used photocatalyst [52]. 'Black TiO_2' is the term that was first coined by Chen et al. in 2011, to characterise defect-induced titanium dioxide, due to its colour change from opaque white to black [52,53]. Electron trapping by surface defects and oxygen vacancy (V_O) sites, and hole trapping by Ti^{3+} sites result in enhanced visible light absorption and reduced charge carrier recombination. Defects can be induced in TiO_2 through a plethora of methods such as metal reduction, ionothermal processes, plasma assisted processes, $NaBH_4$ (sodium borohydride) reduction, microwave radiation, laser ablation, ultrasonication, electrochemical reduction etc [52]. In bismuth titanate, UV irradiation alone was sufficient to induce oxygen vacancies, resulting in significantly increased photocatalytic activity, which means that in practice, one only has to use this photocatalyst to improve its performance [51]. The mechanism behind the oxygen vacancy formation is not yet understood, but Ye et al. attributed it to the low bond energy and long bond length of the Bi−O bond [54].

In the present study, the bismuth titanate photocatalyst was deposited by magnetron sputtering onto glass stirring rods and integrated into a bespoke photocatalytic reactor named LCPR-II for "Low-cost photocatalytic reactor II". The fabrication process did not involve any expensive elements (quartz, membranes, air injector etc.) and relied almost exclusively on components available in the consumer computer market. The design of the present reactor is based on the LCPR-I (Low-cost photocatalytic reactor) [55]. The photocatalytic activity of the reactor was initially evaluated by assessing its ability to degrade methylene blue (MB) under UV-A with a

varying number of coated rods. Then, the durability of the best-performing configuration was assessed through 25 consecutives cycling tests, which progressively turned the coated rods from white to black, as a result of UV induced oxygen vacancies, forming within the bismuth titanate photocatalyst. The pristine bismuth titanate is thus referred to as pBT, while the black bismuth titanate is referred to as bBT. The reactor with the best configuration of black bismuth titanate coated rods was then used to decompose a solution of levofloxacin (LEVO). Levofloxacin is a broad-spectrum antibiotic belonging to the fluoroquinolone group, it is used to treat bacterial infections such as pneumonia, sinusitis, urinary tract infections and gastroenteritis [56]. It is considered an essential medicine by the World Health Organization (WHO) and a reserve antibiotic used to prevent drug resistance when resistant microorganisms are encountered [57].

2. Materials and Methods

2.1. Sample deposition

Bismuth titanate (BT) thin films were deposited using a Nordiko sputtering rig, under a high vacuum, achieved through a combination of rotary (BOC Edwards 80) and turbo molecular (Leybold TMP1000) pumps. Two directly cooled 300x100 mm titanium and bismuth targets (99.5% purity) were fitted, opposite one another, onto Teer Coatings Ltd unbalanced type II magnetrons. The distance between the target and the substrate was kept at 50 mm for all deposition runs, as the substrate were placed on a drum substrate holder, rotated at a speed of 2 rpm. A working pressure of 0.44 Pa was achieved by flowing argon and oxygen gases, both controlled via mass-flow controllers and maintained at 50 and 25 sccm, respectively. The magnetrons were powered by a dual channel Advanced Energy Pinnacle Plus power supply in pulsed DC mode operating at a frequency of 100 kHz and 60% duty. Powers of 750 and 185 W were applied to the titanium and bismuth target, respectively, to achieve the stoichiometry required to deposit $Bi_{12}TiO_{20}$ thin films, based on previous findings [51]. The $Bi_{12}TiO_{20}$ photocatalyst was deposited on the surface of two opposite sides of AR-Glas™ Stirring Rods (length: 250 mm, diameter 6 mm), for 4 h each, over a 250 mm length (purchased from the Fisher). Samples were annealed in air at 600 °C post-deposition for 1 h, to obtain crystalline coatings.

In parallel, soda lime glass microscope slides were coated with bismuth titanate under the same conditions used for the stirring rods, for characterisation purposes. The coating's thickness on the flat samples was estimated to be 0.75 ± 0.4 μm. The flat sample's thickness was measured by creating an artificial step, by covering part of the microscope soda-lime slide with Kapton tape prior to the deposition. A Profilm3D interferometer from Filmetrics, with a magnification of x50, was used to measure the height of the artificial step. Half of the coated microscope slide samples were cycled in the same manner as the rods for characterisation purposes and compared with pristine samples. The photocatalytic pollutant degradation mechanism for both black and white bismuth titanate was studied using a dye degradation test in the presence of different scavengers. To prevent possible self-photosensitization effects due to coloured substance interactions, Orange II was chosen instead of MB [58]. A plane black titanate sample, termed bBT was produced by exposing a flat sample of bismuth titanate to the same treatment as the cycled rods. All the substrates were ultrasonically pre-cleaned in acetone prior to deposition. All chemicals used were purchased from Sigma Aldrich, unless stated otherwise.

The thin film morphology was evaluated by SEM (scanning electron microscopy) using a Zeiss Supra 40 VP-FEG-SEM. The oxidation state information was obtained using XPS (X-ray photoelectron spectroscopy), performed with a SUPRA photoelectron spectrometer (Kratos Analytical Ltd.) equipped with Mg K X-rays as the primary excitation source. A multi-mode gas cluster ion source (GCIS) was used for etching at 20keV with Ar_{50}^{+} clusters for 60 seconds. The binding energy was referenced to the C 1 s line at 284.8 eV for calibration. Curve fitting was performed applying a Gaussian function. The deposited film thickness was measured on a coated soda lime glass slide by creating an artificial step by masking a part of the slide with Kapton tape, prior to deposition. A Profilm3D interferometer from Filmetrics, with a magnification of x50, was used to measure the thickness of the coatings from this step. The crystallinity of the coatings was assessed by XRD (X-ray diffraction), on a Panalytical Xpert system, with Cu Kα 1 radiation at 0.154 nm, in grazing incidence mode at 3° angle of incidence over a scan range from 20 to 70° (2θ), the accelerating voltage and applied current were 40 kV and 30 mA, respectively. The optical band gap of bismuth titanate was estimated using the Tauc plot method, by measuring the optical absorbance of samples produced under the same conditions onto soda lime microscope glass slides [59].

2.2. Photocatalytic reactor

The design of the LCPR-II is based on the LCPR-I developed at the Manchester Metropolitan University earlier [55]. Likewise, the bespoke reactor utilises an external light source and does not involve any costly components (quartz, membranes, air injector etc.); with the exception of the UV-A lamps, the set-up was built exclusively from affordable and readily available parts, purchased from the computer enthusiast market. Contrary to LCPR-I, the present photocatalytic reactor utilises coated glass rods as the photocatalyst. Additionally, TiO_2 was substituted with bismuth titanate, a more efficient and promising photocatalyst [51]. Figure 1 provides a schematic representation of the bespoke water treatment photocatalytic reactor loaded with bismuth titanate coated glass stirring rods and a photograph of the separate components.

In brief, the system is comprised of a cylindrical reactor made from PMMA (polymethylmethacrylate), transparent PVC (polyvinyl chloride) tubing, a 12 V pump, a flowmeter, a temperature probe and an acrylic analysis cell. The reactor was placed in an aluminium enclosure with a UV-A irradiation source. The pump was operated at minimum capacity, to minimise power consumption, without limiting mass transfer, resulting in a flowrate of 5.14 $L.min^{-1}$ [55]. Increasing the number of coated glass rods increases the catalyst load, and by extension the reaction rate, up to a certain point where light would be blocked, and performances would stop increasing. To find the best conditions, the reactor was loaded with 4 to 10 glass rods, with 2 rods increments, coated on two opposite sides with bismuth titanate, by reactive magnetron sputtering. A full breakdown of the upfront price of the LCPR-II is given in Table 1. The power drawn by the system was measured directly at the wall with a wattmeter and remained below 60 W.

Table 1. Cost summary for LCPR-II.

Component	Material	Price[1]		
		£	€	$
Reactor[2]	PMMA	15.5	18.1	21.6
Tubing[3]	PVC	12.7	14.9	17.7
Flowmeter	Aluminium allow + POM	36.9	43.2	51.4

Temperature probe	Aluminium alloy	19.0	22.2	26.5
Sampling cell	Acrylic	5.7	6.7	7.9
AR-Glas™ Stirring Rods (× 10)	Glass	5.3	6.1	7.3
Pump	Acrylic	31.8	37.2	44.3
Miscellaneous	-	30.0	35.1	41.8
UVP XX-15 Series UV Bench Lamp	Aluminium	229.5	268.5	319.5
Total (without light source)		**156.9**	**183.5**	**218.4**
Total (with light source)		**386.4**	**452.0**	**537.9**
[1]as at 15th of March 2021	[2]Outer diameter: 5 cm Height: 24 cm	[3] Outer diameter: 16 mm Inner diameter: 10 mm		

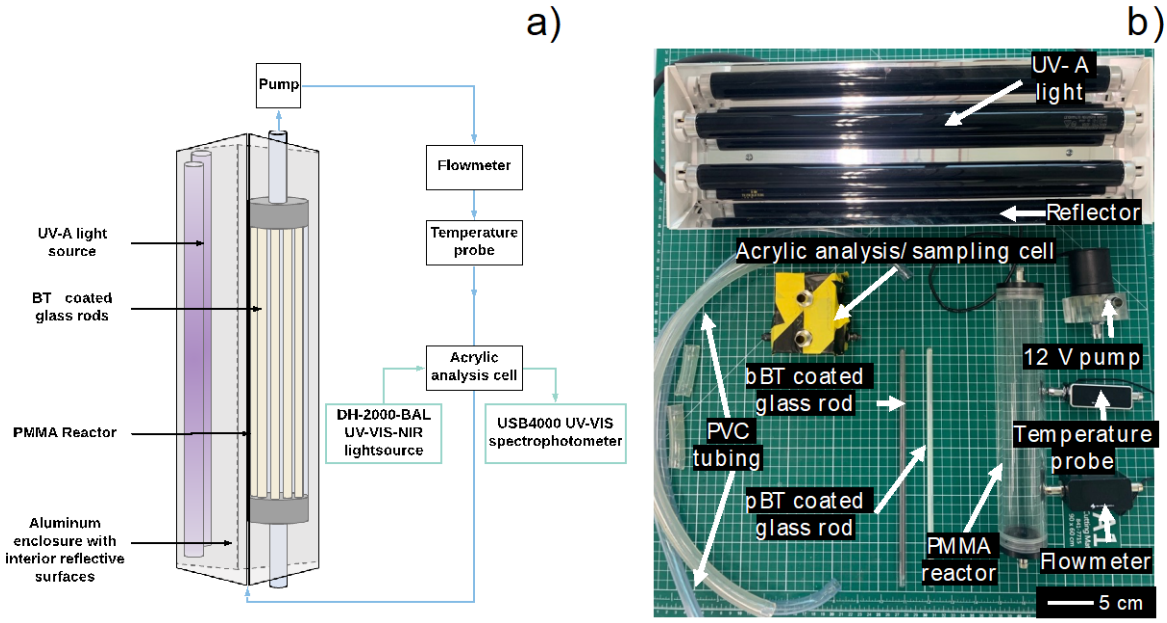

Figure 1. LCPR-II a) schematic representation of LCPR-II, b) picture of disassembled LCPR-II.

2.3. Photocatalytic reactor optimisation

The photocatalytic performance of the bespoke water treatment reactor was assessed by monitoring its ability to degrade methylene blue under UV-A light. The reactor was filled with an aqueous methylene blue solution, purchased from Alfa Aesar, of 500 mL at a concentration of 1 µmol.L^{-1}. MB degradation tests were first carried out with a varying number of pBT coated rods (4, 6, 8 and 10), to identify the configuration that would yield the best photocatalytic activity. A test without any rods and with 4 uncoated rods was also carried out as controls to account for photolysis. The reactor was left in the dark at room temperature for 1 h under continuous solution circulation to reach adsorption-desorption equilibrium. Once reached, the UV-A source (Sankyo Denki BLB lamps, peak output at 365 nm) was powered up for 4 h. The methylene blue main absorption peak at 664 nm was monitored every 10 min with an Ocean Optics USB4000 UV-visible spectrometer. Between each test, both the pBT coated glass rods and the reactor were thoroughly rinsed with distilled water. The reactor's photocatalytic degradation efficiency was calculated using equation (1) and used as a response to optimise the photocatalytic

degradation process, with A_0 and A_t as MB's main absorbance peak at 664 nm at 0 and 5 h of UV irradiation, respectively.

$$(1) \qquad MB\ removal\ (\%) = \frac{A_0 - A_t}{A_0} \times 100$$

2.4. Reusability assessment

To evaluate the durability and reusability of the coated rods, 25 consecutive MB removal tests were performed with the most efficient configuration (10 pBT coated rods), using the same photocatalytic activity assessment methodology. The time required to degrade 90 % of the initial MB concentration ($\tau_{90\%}$) under UV-A was used as a response to evaluate the durability of photocatalytic reactor.

2.5. Scavenger experiment

Bismuth titanate and black bismuth titanate samples on flat glass slides were tested for their ability to degrade Orange II, in the presence of different scavengers. The following trapping agents were employed: isopropanol [42,60,61] for $^{\bullet}OH$, 4-hydroxy TEMPO [42,62] for $O_2^{\bullet -}$, sodium oxalate [28,63] for h^+ and sodium nitrate [64] for e^-. Methylene blue could not be used, because it has a complementary colour to 4-hydroxy TEMPO; it forms a green solution when mixed. Thus, to prevent possible self-photosensitization effects due to coloured substance interactions, Orange II was chosen instead [58]. Samples were placed on top of a sample holder in a quartz cuvette, immersed in a 50 mL solution of Orange II (2 μmol/L) in the presence of each scavenger (7 mmol/L). The samples were left in the dark for 30 minutes under continuous stirring, to reach adsorption-desorption equilibrium and then irradiated by the same UV-A light source used for LCPR-II. The main absorption peak of Orange II (500 nm) was monitored with an Ocean Optics USB4000 UV–vis spectrometer.

2.6. Antibiotic degradation experiment

LCPR-II was used to decompose a 500 mL solution of levofloxacin (LEVO), purchased from Sigma Aldrich, with a concentration of 10 mg.L^{-1}. The reactor was loaded with 10 cycled bBT coated glass rods and irradiated under UV-A for 24 h. As a control, the same experiment was carried out without any rods under the same conditions. 10 mL of solution were sampled at times 0 and 24 h for both the catalyst loaded reactor and the control. The absorbance spectra of the untreated and treated solutions were obtained using an Agilent Cary 300 UV–vis spectrophotometer. The degradation of LEVO was further investigated by testing the antimicrobial activity of treated and untreated solutions, against *Escherichia coli* ATCC 8739 (EC), *Staphylococcus aureus* ATCC 6538 (SA) and *Acinetobacter baumannii* ATCC 19606 (AB). Bacteria were grown overnight in TSB media, which were then inoculated onto agar plates (100 μL) using the spread plate method. Filter-paper disks (9mm diameter) were impregnated with a 20 μL solution of either distilled water (as a control), initial LEVO solution, LEVO treated solution under UV without the coated rods and LEVO treated solution under UV with the coated rods. As the solutions diffuse from the filter-paper disk onto the agar, they may kill the bacteria or stop them from growing. If this is the case, an area around the disk will form, as bacteria cannot grow and multiply enough to be visible. This area is called "zone of inhibition" and its diameter was measured to compare the effectiveness of the different treatments. Experiments were performed in triplicate to obtain an average diameter measurement.

3. Results and discussion

3.1. Photocatalytic reactor optimisation

As displayed in Figure 2a, when the reactor was loaded with 4, 6, 8 and 10 rods, after 240 minutes of UV-A irradiation, it achieved MB removal percentages of 40, 59, 75 and 89 %, respectively. In the control experiment, residual adsorption and photolysis accounted for less than 10 % of the dye discoloration. This result was expected as increasing the number of rods, ultimately increased the photocatalyst loading. Even when using 10 rods, light blocking didn't impact negatively the reaction rate. Additional coated rods couldn't be added to the reactor in its current configuration, but future work will be aimed at further increasing the number of coated rods.

The LCPR-II reusability was assessed with the best performing configuration (10 rods) by conducting 25 consecutive MB degradation test cycles with 240 min of UV-A irradiation (Figure 2b). The time required to decompose 90 % of the model pollutant ($\tau_{90\%}$) was estimated for each cycle. Between the first and last test, $\tau_{90\%}$ decreased from 4 to about 1 hour, while the colour of the pBT coated rods changed from white to black. This behaviour was previously reported for bismuth titanate, as a result of oxygen vacancies forming when exposed to UV-A [51]. These vacancies act as trapping sites for electrons, prolonging their lifetime and improving the photocatalytic activity of the catalyst.

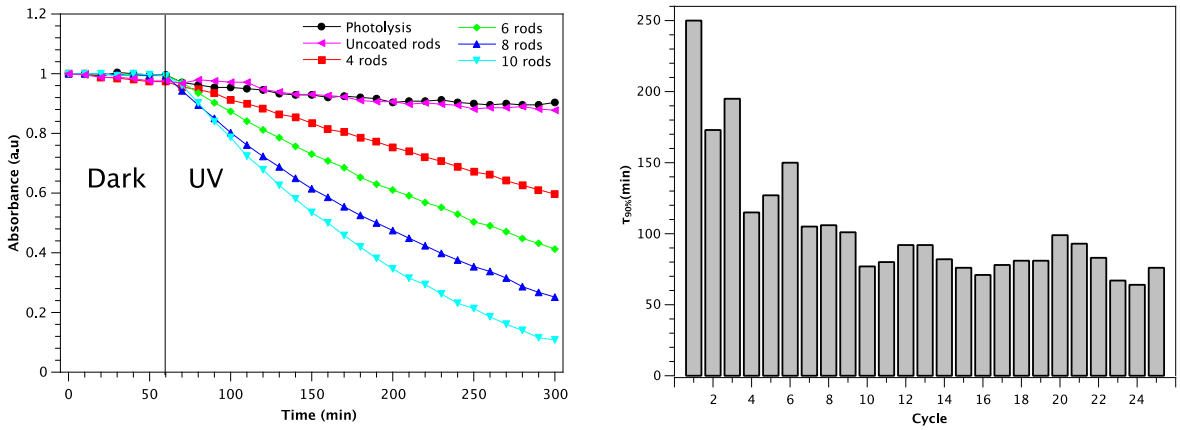

Figure 2. MB degradation tests results a) Varying number of pBT-coated rods, b) cycling experiment with 10 coated rods.

3.2. Investigation of Black bismuth titanate properties

The optical band gap energy of the crystalline semiconductors was estimated using the Tauc plot method [59], by plotting $(\alpha h\nu)^{1/2}$ as a function of $h\nu$ and extrapolating the linear region to the abscissa (where α is the absorbance coefficient, h is Plank's constant, ν is the frequency of vibration). Although the cycling experiment resulted in a colour change, no significant change in the band gap was observed. Bandgap energy values were estimated at 2.69 and 2.71 eV for pBT and bBT, respectively (Figure 3).

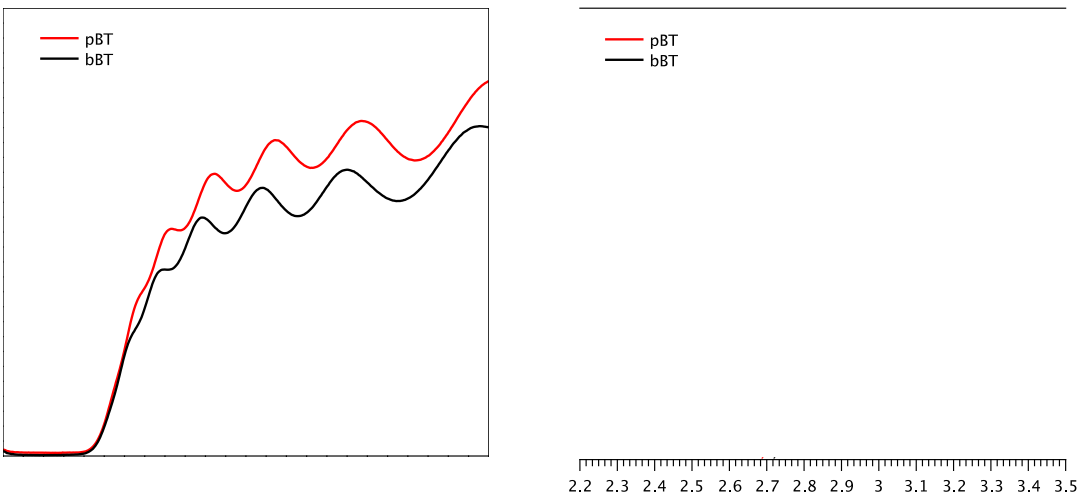

Figure 3. UV-Vis absorption spectra for pBT and bBT samples a) and corresponding Tauc plots b).

XRD analysis didn't reveal any crystalline change between pristine bismuth titanate and black bismuth titanate (Figure 5), in both cases cubic (I23) $Bi_{12}TiO_{20}$ was identified (ICDD 96-403-0657). Crystalline peaks belonging to the cubic fphase were identified at 2θ of 21.3° (121), 24.7° (022), 27.6° (013), 30.3° (222), 32.8° (123), 35.2° (040), 37.4° (033), 39.5° (042), 41.5° (233), 43.4° (242), 45.3° (143), 48.9° (125), 52.2° (053), 53.9° (060), 55.5° (235) and 58.6° (145). The results of the band gap and crystalline phase analysis are consistent with the findings of an earlier study investigating the properties of a $Bi_{12}TiO_{20}/Bi_4Ti_3O_{12}$ photocatalyst [51].

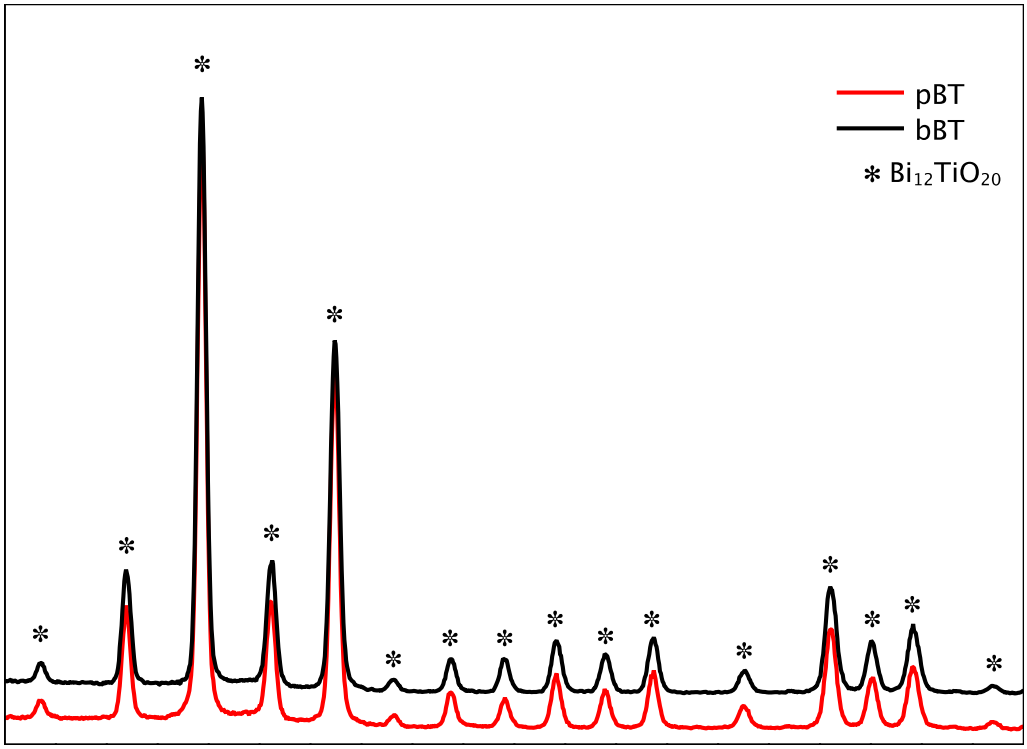

Figure 4. XRD analysis of a) pristine bismuth titanate and b) black bismuth titanate.

High-resolution O 1s XPS spectra of pBT and bBT samples are shown in Figure 5, both O 1s peaks can be deconvoluted into 5 peaks. The first two deconvoluted peaks at 529.4 and 530.9 eV were attributed to lattice and vacancy oxygen species, respectively [51]. The three following deconvoluted peaks at 533.6, 541.7 and 532.5 eV can be attributed to adsorbed organic species ($C = O$, $C - O$, $O - C = O$). As expected, when compared to the pristine bismuth titanate sample (Figure 5a), black bismuth titanate (Figure 5b) has a higher proportion of adsorbed organic species as a result of the methylene blue degradation cycling tests. Interestingly, the black bismuth titanate sample also has a lower atomic percentage ratio of O 1s L to O 1s V species (from relative areas of the peaks), changed from ca. 4.4:1 to ca. 1.8:1 for the pBT and bBT samples, respectively. Oxygen vacancies induced by UV light irradiation have already been reported for bismuth titanate coatings; these defects, have been shown to increase the lifetime of photogenerated species, leading to a significantly improved photocatalytic activity [51]. Depth profiling analysis didn't reveal any difference between the pristine and black bismuth titanate, in both cases only the lattice oxygen peak was present.

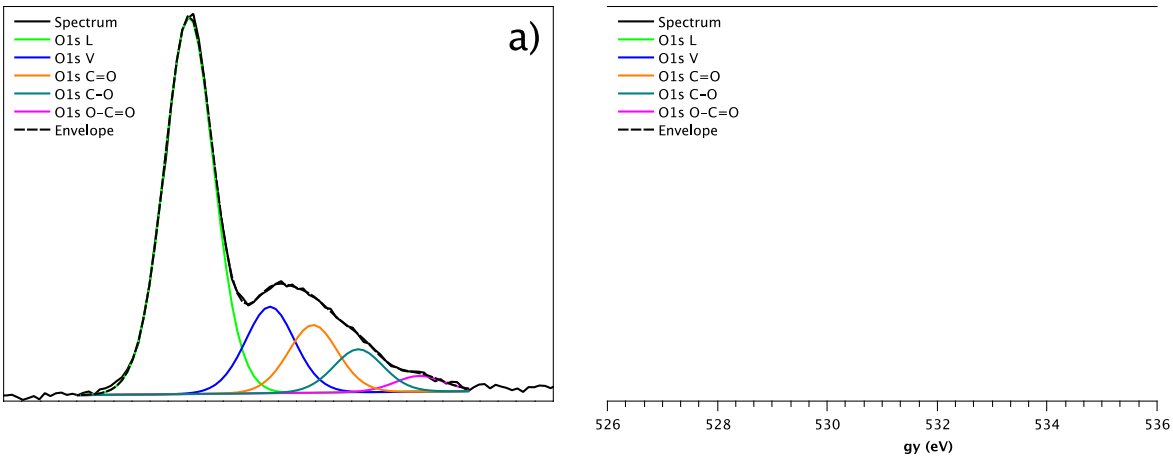

Figure 5. High-resolution O1s XPS spectra of a) pBT and b) bBT samples.

SEM micrographs of the samples didn't reveal any morphological difference between pristine (Figure 6a) and black bismuth titanate (Figure 6b). The surface of the black bismuth titanate sample appears a bit rougher, but this is most likely due to the cycling of the sample which was covered with organic contaminants that couldn't be washed off with distilled water. The EDX analysis didn't reveal any significant change, with a Bi, Ti and O atomic percentage content of 37.1 ± 0.4, 3.5 ± 0.4 and 59.4 ± 0.1 % for pristine pBT and 34.9 ± 0.5, 3.1 ± 0.3 and 62.0 ± 0.2 % for bBT, respectively.

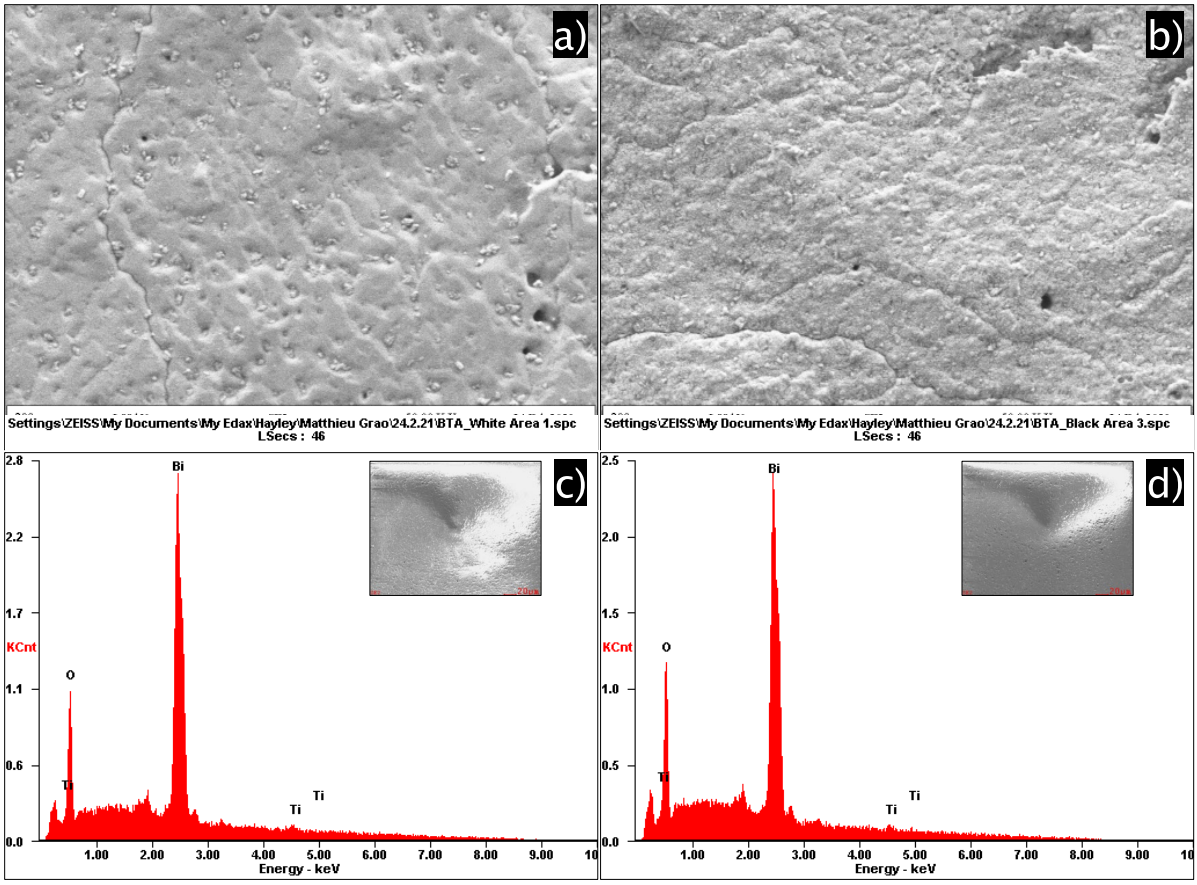

Figure 6. Surface SEM micrographs of samples a) pBT, b) bBT; EDX analysis of samples c) pBT, d) pBT.

3.3. Photocatalytic degradation mechanism investigation

To understand the mechanism behind the photocatalytic degradation of pollutants, pBT and bBT flat samples were used to decompose Orange II under UV-A, in the presence of different trapping agents. 4 hydroxy-TEMPO was used to scavenge superoxide radicals, isopropanol for hydroxyl radicals, sodium oxalate for holes and sodium nitrate for electrons. In the case of pBT (Figure 7a), sodium oxalate and 4 hydroxy-TEMPO reduced significantly the photocatalyst's activity, with the latter having a greater effect, while sodium nitrate and isopropanol didn't slow down the reaction. Consequently, superoxide radicals ($O_2^{-\bullet}$) and, to a lesser extent, holes (h^+) appear to be the main driving force behind the photocatalytic activity of bismuth titanate. This is consistent with the findings of Guo et al. who reported that h^+ and $O_2^{-\bullet}$ are the main active species [65]. When testing bBT (Figure 7b), not only did sodium oxalate and 4 hydroxy-TEMPO reduce significantly the photocatalytic activity of black bismuth titanate, but so did sodium nitrate. In ascending order of contribution, superoxide radicals ($O_2^{-\bullet}$), electrons (e^-) and holes (h^+) were the main driving force behind the photocatalytic degradation process. This is in accordance with the earlier results of the XPS analysis [45], which revealed the presence of an increased amount of oxygen vacancies (V_o) in black bismuth titanate, when compared to the pristine one. These oxygen vacancies (V_o) are likely to act as trapping sites for electrons (e^-), increasing their lifetime and likelihood of reacting with the pollutant at the photocatalyst's surface. The proposed photocatalytic pollutant degradation mechanism in pristine and black bismuth titanate is illustrated in Figure 8.

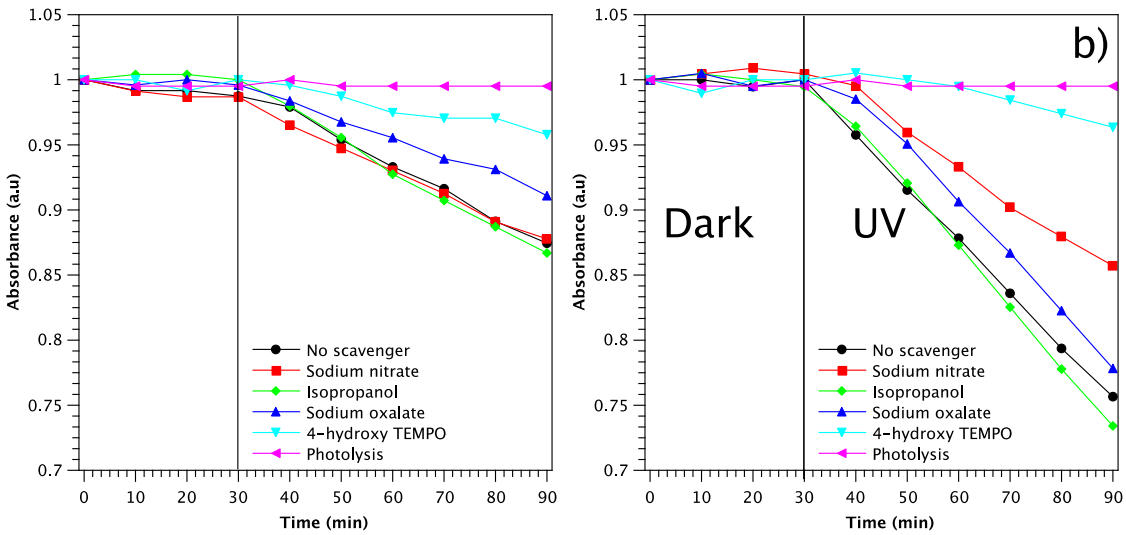

Figure 7. Orange II (2μmol/L) degradation under UV-A irradiation by in the presence of h^+, e^-, $O_2^{\bullet-}$ and $^\bullet OH$ scavengers by a) pBT and b) bBT.

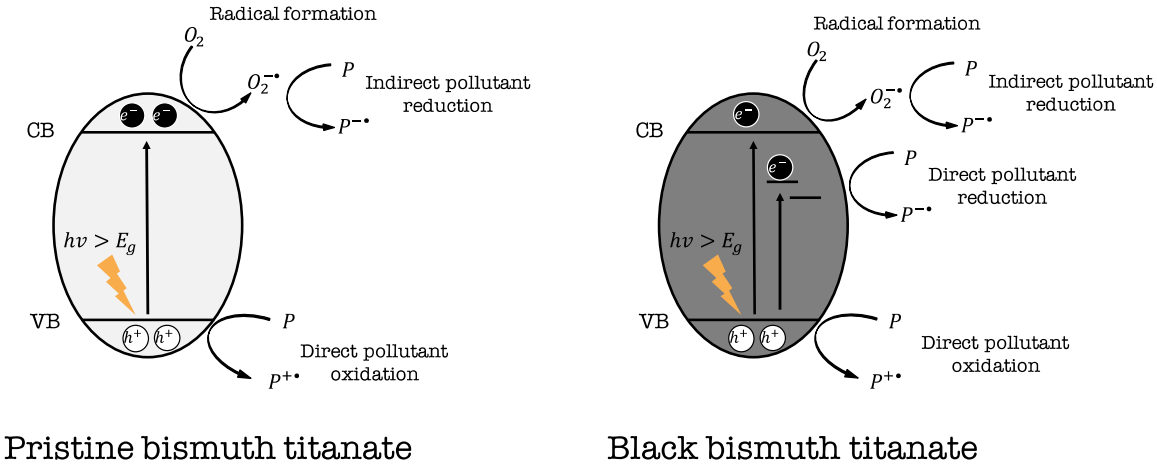

Figure 8. Schematic of proposed photocatalysis mechanism in pristine and black bismuth titanate.

3.4. Photocatalytic degradation test of antibiotic

The capabilities of LCPR-II were tested against levofloxacin (LEVO), an antibiotic commonly found in wastewater treatment plant effluents. The reactor was loaded with a 500 mL solution at a concentration of 10 mg.L^{-1}. After 24 h of UV light irradiation without the coated rods (Figure 9a), only a slight decrease in the LEVO main absorbance peak at 287.5 nm was observed by UV-Vis spectroscopy. Alternatively, when the black bismuth titanate coated rods were included (Figure 9b), the main absorbance peak was evidently not present. Broad absorbance peaks appeared between 200 and 280 nm, which may be attributed to the formation of different reaction intermediates during the photocatalytic degradation process. To assess the antimicrobial properties of the treated solutions, disk diffusions tests were performed with samples from the initial and treated LEVO solutions. Both the initial and the UV-only treated LEVO solutions demonstrated antibiotic activity, with a clear zone of inhibition forming around each corresponding disc (Figure 9c). On the other hand, no inhibition zone was identified when the solution was treated with UV in the presence of black bismuth titanate coated rods (Figure 9c). The same result was found for the distilled water control. In the UV-only treated solution, a 20 % reduction in inhibition zone diameter was observed for *S. aureus* and *A. baumannii* (Figure 9d). The UV was most likely able to degrade a small amount of LEVO. This effect was not observed in *E. coli* cultures, as they appear considerably more sensitive to the levofloxacin, with an inhibition zone diameter 30 % and 20 % larger, on average, than the ones measured for *S. aureus* and *A. baumannii*, respectively. These results confirm that the photocatalytic reactor was able to degrade the levofloxacin and that the reaction intermediates are innocuous to the tested microorganisms.

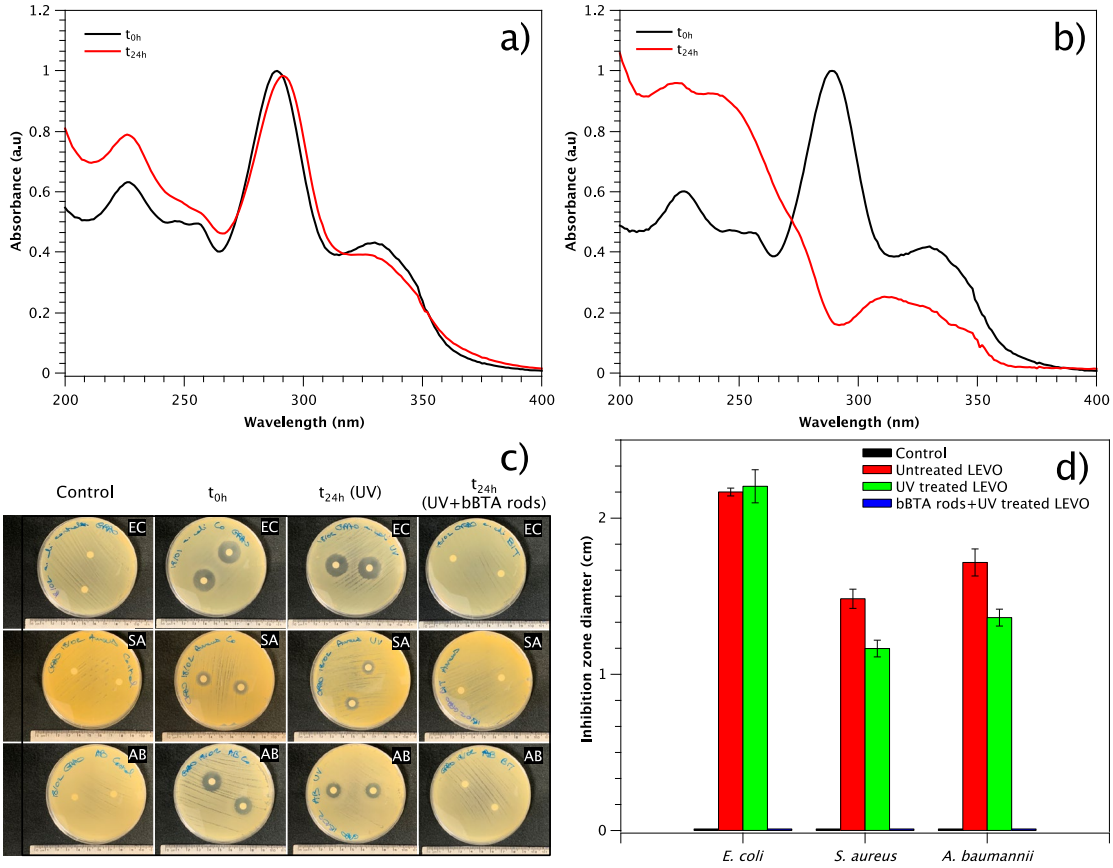

Figure 9. Levofloxacin (LEVO) degradation experiment a) UV-Vis spectrum of UV-A treated LEVO, b) UV-Vis spectrum of bBT treated LEVO under UV-A, c) pictures of pathogens exposed to treated LEVO solutions (EC: E. coli, SA: S. aureus, AB: A. baumannii), d) inhibition zone diameter measurements.

Although it took the LCPR-II 24 h to decompose the levofloxacin, one should keep in mind that the tested concentration far exceeded the concentration of antibiotics sampled in wastewater treatment effluents by a factor of 10^3 to 10^6. In photocatalysis, initial pollutant concentration is a significant contributor to the reaction rate, the lower the concentration, the faster the reaction. Other authors were able to decompose levofloxacin in a shorter amount of time [66–69], however, these photocatalysts were produced in powder-form. Powder form photocatalysts are inherently more active due to their high specific surface area, but they require post-process separation to safely discard the treated water, which hinders scalability [70]. Furthermore, when the reactor was loaded with coated rods, it outperformed the "UV only" treatment, which is typically used as a last disinfection steps in wastewater treatment plants [7]. The results of this proof-of-concept highlight the potential of bismuth titanate coated rods, to improve the removal and inhibition of pollutants, such as antibiotics, through photocatalysis. We believe that developing an affordable, sustainable, efficient and scalable wastewater treatment reactor is a step in the right direction towards the adoption of photocatalytic systems in treatment plants.

4. Conclusion

In the present study, a bespoke photocatalytic reactor was built from consumer market equipment and loaded with glass stirring rods coated with bismuth titanate by reactive magnetron sputtering. When loaded with 10 coated rods, the reactor proved effective at decomposing 90 %

of an aqueous methylene blue solution, under UV-A, in 4 hours. During the reusability assessment, equivalent to 125 h of consecutive use, the time required to decompose 90 % of the pollutant, with the same concentration, dropped from 4 to 1 hour. This remarkable property is due to photoinduced vacancies, acting as electron trapping sites, and is characterised by a photocatalyst colour change from white to black. In pristine bismuth titanate coatings, superoxide ($O_2^{\cdot -}$) and holes (h^+), were identified as the main drivers of the photocatalytic activity. Interestingly, in black bismuth titanate, superoxide ($O_2^{\cdot -}$) and holes (h^+) were not the only contributors, as electrons (e^-) also played a significant role. This last contribution is most likely due to the presence of newly formed oxygen vacancies, acting as traps and increasing the photocatalytic activity. Finally, the reactor was able to successfully degrade a concentrated solution of levofloxacin, whose antimicrobial potency was assessed by inhibition zone tests in the presence of *E. coli*, *S. aureus* and *A. baumannii*. This study demonstrates the potential of bismuth titanate based photocatalytic reactors for downstream wastewater treatment. This system could be used complementarily to UV disinfection, to decompose remaining traces of pollutants, to prevent the spread of antibiotic resistant bacteria in wastewaters.

CRediT authorship contribution statement

Matthieu Grao: Conceptualization, Methodology, Software, Validation, Investigation, Visualization. James Redfern: Methodology, Validation. Peter J Kelly: Resources, Supervision, Funding acquisition. Marina Ratova: Conceptualization, Validation, Supervision, Project administration.

Funding

This research did not receive any specific grant from funding agencies in the public, commercial, or not-for-profit sectors.

References

[1] N.L. Nemerow, Industrial Waste Treatment: Contemporary Practice and Vision for the Future, Elsevier, 2010.

[2] WHO | Progress on drinking water, sanitation and hygiene, WHO. (n.d.). http://www.who.int/water_sanitation_health/publications/jmp-2017/en/ (accessed October 10, 2018).

[3] Antimicrobial resistance, (n.d.). https://www.who.int/news-room/fact-sheets/detail/antimicrobial-resistance (accessed March 4, 2021).

[4] B.W.N. Grehs, M.A.O. Linton, B. Clasen, A. de Oliveira Silveira, E. Carissimi, Antibiotic resistance in wastewater treatment plants: understanding the problem and future perspectives, Arch. Microbiol. (2020). https://doi.org/10.1007/s00203-020-02093-6.

[5] J. Blázquez, A. Couce, J. Rodríguez-Beltrán, A. Rodríguez-Rojas, Antimicrobials as promoters of genetic variation, Curr. Opin. Microbiol. 15 (2012) 561–569. https://doi.org/10.1016/j.mib.2012.07.007.

[6] A. Rodríguez-Rojas, J. Rodríguez-Beltrán, A. Couce, J. Blázquez, Antibiotics and antibiotic resistance: A bitter fight against evolution, Int. J. Med. Microbiol. 303 (2013) 293–297. https://doi.org/10.1016/j.ijmm.2013.02.004.

[7] C.M. Manaia, J. Rocha, N. Scaccia, R. Marano, E. Radu, F. Biancullo, F. Cerqueira, G. Fortunato, I.C. Iakovides, I. Zammit, I. Kampouris, I. Vaz-Moreira, O.C. Nunes, Antibiotic resistance in wastewater treatment plants: Tackling the black box, Environ. Int. 115 (2018) 312–324. https://doi.org/10.1016/j.envint.2018.03.044.

[8] M. Yasojima, N. Nakada, K. Komori, Y. Suzuki, H. Tanaka, Occurrence of levofloxacin, clarithromycin and azithromycin in wastewater treatment plant in Japan, Water Sci. Technol. J. Int. Assoc. Water Pollut. Res. 53 (2006) 227–233. https://doi.org/10.2166/wst.2006.357.

[9] A.C. Johnson, M.D. Jürgens, N. Nakada, S. Hanamoto, A.C. Singer, H. Tanaka, Linking changes in antibiotic effluent concentrations to flow, removal and consumption in four different UK sewage treatment plants over four years, Environ. Pollut. 220 (2017) 919–926. https://doi.org/10.1016/j.envpol.2016.10.077.

[10] R.H. Lindberg, P. Wennberg, M.I. Johansson, M. Tysklind, B.A.V. Andersson, Screening of Human Antibiotic Substances and Determination of Weekly Mass Flows in Five Sewage Treatment Plants in Sweden, Environ. Sci. Technol. 39 (2005) 3421–3429. https://doi.org/10.1021/es048143z.

[11] I. Senta, S. Terzic, M. Ahel, Occurrence and fate of dissolved and particulate antimicrobials in municipal wastewater treatment, Water Res. 47 (2013) 705–714. https://doi.org/10.1016/j.watres.2012.10.041.

[12] E. Gracia-Lor, J.V. Sancho, F. Hernández, Multi-class determination of around 50 pharmaceuticals, including 26 antibiotics, in environmental and wastewater samples by ultra-high performance liquid chromatography–tandem mass spectrometry, J. Chromatogr. A. 1218 (2011) 2264–2275. https://doi.org/10.1016/j.chroma.2011.02.026.

[13] L. Gao, Y. Shi, W. Li, H. Niu, J. Liu, Y. Cai, Occurrence of antibiotics in eight sewage treatment plants in Beijing, China, Chemosphere. 86 (2012) 665–671. https://doi.org/10.1016/j.chemosphere.2011.11.019.

[14] L. Birošová, T. Mackuľak, I. Bodík, J. Ryba, J. Škubák, R. Grabic, Pilot study of seasonal occurrence and distribution of antibiotics and drug resistant bacteria in wastewater treatment plants in Slovakia, Sci. Total Environ. 490 (2014) 440–444. https://doi.org/10.1016/j.scitotenv.2014.05.030.

[15] S. Rodriguez-Mozaz, I. Vaz-Moreira, S. Varela Della Giustina, M. Llorca, D. Barceló, S. Schubert, T.U. Berendonk, I. Michael-Kordatou, D. Fatta-Kassinos, J.L. Martinez, C. Elpers, I. Henriques, T. Jaeger, T. Schwartz, E. Paulshus, K. O'Sullivan, K.M.M. Pärnänen, M. Virta, T.T. Do, F. Walsh, C.M. Manaia, Antibiotic residues in final effluents of European wastewater treatment plants and their impact on the aquatic environment, Environ. Int. 140 (2020) 105733. https://doi.org/10.1016/j.envint.2020.105733.

[16] A. Fujishima, K. Honda, Electrochemical photolysis of water at a semiconductor electrode, Nature. 238 (1972) 37–38.

[17] A. Atli, A. Atilgan, A. Yildiz, Multi-layered TiO2 photoanodes from different precursors of nanocrystals for dye-sensitized solar cells, Sol. Energy. 173 (2018) 752–758. https://doi.org/10.1016/j.solener.2018.08.027.

[18] R. Bendoni, N. Sangiorgi, A. Sangiorgi, A. Sanson, Role of water in TiO2 screen-printing inks for dye-sensitized solar cells, Sol. Energy. 122 (2015) 497–507. https://doi.org/10.1016/j.solener.2015.09.025.

[19] S. Shiva Kumar, S.U.B. Ramakrishna, S.V. Krishna, K. Srilatha, B.R. Devi, V. Himabindu, Synthesis of titanium (IV) oxide composite membrane for hydrogen production through alkaline water electrolysis, South Afr. J. Chem. Eng. 25 (2018) 54–61. https://doi.org/10.1016/j.sajce.2017.12.004.

[20] D. Chen, Z. Liu, Z. Guo, W. Yan, M. Ruan, Decorating Cu2O photocathode with noble-metal-free Al and NiS cocatalysts for efficient photoelectrochemical water splitting by light

harvesting management and charge separation design, Chem. Eng. J. 381 (2020) 122655. https://doi.org/10.1016/j.cej.2019.122655.
[21]Y. Won, K. Schwartzenberg, K.A. Gray, TiO2-based transparent coatings create self-cleaning surfaces, Chemosphere. 208 (2018) 899–906. https://doi.org/10.1016/j.chemosphere.2018.06.014.
[22]J. Singh, S. Jadhav, S. Avasthi, P. Sen, Designing Photocatalytic Nanostructured Antibacterial Surfaces: Why Is Black Silica Better than Black Silicon?, ACS Appl. Mater. Interfaces. 12 (2020) 20202–20213. https://doi.org/10.1021/acsami.0c02854.
[23]M. Grao, C. Amorim, R. Brito Portela Marcelino, P. Kelly, Crystalline TiO2 supported on stainless steel mesh deposited in a one step process via pulsed DC magnetron sputtering for wastewater treatment applications, J. Mater. Res. Technol. 9 (2020) 5761–5773. https://doi.org/10.1016/j.jmrt.2020.03.101.
[24]H. Anwer, A. Mahmood, J. Lee, K.-H. Kim, J.-W. Park, A.C.K. Yip, Photocatalysts for degradation of dyes in industrial effluents: Opportunities and challenges, Nano Res. 12 (2019) 955–972. https://doi.org/10.1007/s12274-019-2287-0.
[25]M. Asiltürk, F. Sayılkan, E. Arpaç, Effect of Fe3+ ion doping to TiO2 on the photocatalytic degradation of Malachite Green dye under UV and vis-irradiation, J. Photochem. Photobiol. Chem. 203 (2009) 64–71. https://doi.org/10.1016/j.jphotochem.2008.12.021.
[26]E. Bilgin Simsek, Solvothermal synthesized boron doped TiO2 catalysts: Photocatalytic degradation of endocrine disrupting compounds and pharmaceuticals under visible light irradiation, Appl. Catal. B Environ. 200 (2017) 309–322. https://doi.org/10.1016/j.apcatb.2016.07.016.
[27]R. Janssens, M.K. Mandal, K.K. Dubey, P. Luis, Slurry photocatalytic membrane reactor technology for removal of pharmaceutical compounds from wastewater: Towards cytostatic drug elimination, Sci. Total Environ. 599–600 (2017) 612–626. https://doi.org/10.1016/j.scitotenv.2017.03.253.
[28]N. Liu, Q. Zhu, N. Zhang, C. Zhang, N. Kawazoe, G. Chen, N. Negishi, Y. Yang, Superior disinfection effect of Escherichia coli by hydrothermal synthesized TiO2-based composite photocatalyst under LED irradiation: Influence of environmental factors and disinfection mechanism, Environ. Pollut. 247 (2019) 847–856. https://doi.org/10.1016/j.envpol.2019.01.082.
[29]J. Redfern, M. Ratova, A.P. Dean, J. Pritchett, M. Grao, J. Verran, P. Kelly, Visible light photocatalytic bismuth oxide coatings are effective at suppressing aquatic cyanobacteria and degrading free-floating genomic DNA, J. Environ. Sci. 104 (2021) 128–136. https://doi.org/10.1016/j.jes.2020.11.024.
[30]M. Ratova, J. Redfern, J. Verran, P.J. Kelly, Highly efficient photocatalytic bismuth oxide coatings and their antimicrobial properties under visible light irradiation, Appl. Catal. B Environ. 239 (2018) 223–232. https://doi.org/10.1016/j.apcatb.2018.08.020.
[31]M. Abdennouri, M. Baâlala, A. Galadi, M. El Makhfouk, M. Bensitel, K. Nohair, M. Sadiq, A. Boussaoud, N. Barka, Photocatalytic degradation of pesticides by titanium dioxide and titanium pillared purified clays, Arab. J. Chem. 9 (2016) S313–S318. https://doi.org/10.1016/j.arabjc.2011.04.005.
[32]S. Ahmed, M.G. Rasul, R. Brown, M.A. Hashib, Influence of parameters on the heterogeneous photocatalytic degradation of pesticides and phenolic contaminants in wastewater: A short review, J. Environ. Manage. 92 (2011) 311–330. https://doi.org/10.1016/j.jenvman.2010.08.028.
[33]C. Byrne, G. Subramanian, S.C. Pillai, Recent advances in photocatalysis for environmental applications, J. Environ. Chem. Eng. 6 (2018) 3531–3555. https://doi.org/10.1016/j.jece.2017.07.080.

[34]M. Ratova, R. Klaysri, P. Praserthdam, P.J. Kelly, Visible light active photocatalytic C-doped titanium dioxide films deposited via reactive pulsed DC magnetron co-sputtering: Properties and photocatalytic activity, Vacuum. 149 (2018) 214–224. https://doi.org/10.1016/j.vacuum.2018.01.003.
[35]M. Bernareggi, G.L. Chiarello, G. West, M. Ratova, A.M. Ferretti, P. Kelly, E. Selli, Cu and Pt clusters deposition on TiO2 powders by DC magnetron sputtering for photocatalytic hydrogen production, Catal. Today. 326 (2019) 15–21. https://doi.org/10.1016/j.cattod.2018.07.011.
[36]B. Pongthawornsakun, P. Kaewsuanjik, P. Kittipreechakun, M. Ratova, P. Kelly, O. Mekasuwandumrong, P. Praserthdam, J. Panpranot, Deposition of Pt nanoparticles on TiO2 by pulsed direct current magnetron sputtering for selective hydrogenation of vanillin to vanillyl alcohol, Catal. Today. 358 (2020) 51–59. https://doi.org/10.1016/j.cattod.2019.08.045.
[37]O. Mekasuwandumrong, N. Jantarasorn, J. Panpranot, M. Ratova, P. Kelly, P. Praserthdam, Synthesis of Cu/TiO2 catalysts by reactive magnetron sputtering deposition and its application for photocatalytic reduction of CO2 and H2O to CH4, Ceram. Int. 45 (2019) 22961–22971. https://doi.org/10.1016/j.ceramint.2019.07.340.
[38]I. Suhariadi, M. Shiratani, N. Itagaki, Morphology Evolution Of ZnO Thin Films Deposited By Nitrogen Mediated Crystallization Method, MATEC Web Conf. 159 (2018) 02008. https://doi.org/10.1051/matecconf/201815902008.
[39]Z. Shi, P. Xu, X. Shen, Y. Zhang, L. Luo, G. Duoerkun, L. Zhang, TiO2/MoS2 heterojunctions-decorated carbon fibers with broad-spectrum response as weaveable photocatalyst/photoelectrode, Mater. Res. Bull. 112 (2019) 354–362. https://doi.org/10.1016/j.materresbull.2019.01.005.
[40]J.C. Medina, N.S. Portillo-Vélez, M. Bizarro, A. Hernández-Gordillo, S.E. Rodil, Synergistic effect of supported ZnO/Bi2O3 heterojunctions for photocatalysis under visible light, Dyes Pigments. 153 (2018) 106–116. https://doi.org/10.1016/j.dyepig.2018.02.006.
[41]K.K. Bera, R. Majumdar, M. Chakraborty, S.K. Bhattacharya, Phase control synthesis of α, β and α/β Bi2O3 hetero-junction with enhanced and synergistic photocatalytic activity on degradation of toxic dye, Rhodamine-B under natural sunlight, J. Hazard. Mater. 352 (2018) 182–191. https://doi.org/10.1016/j.jhazmat.2018.03.029.
[42]W. Zhao, Y. Feng, H. Huang, P. Zhou, J. Li, L. Zhang, B. Dai, J. Xu, F. Zhu, N. Sheng, D.Y.C. Leung, A novel Z-scheme Ag3VO4/BiVO4 heterojunction photocatalyst: Study on the excellent photocatalytic performance and photocatalytic mechanism, Appl. Catal. B Environ. 245 (2019) 448–458. https://doi.org/10.1016/j.apcatb.2019.01.001.
[43]L. Zhang, W. Wang, L. Zhou, H. Xu, Bi2WO6 Nano- and Microstructures: Shape Control and Associated Visible-Light-Driven Photocatalytic Activities, Small. 3 (2007) 1618–1625. https://doi.org/10.1002/smll.200700043.
[44]W.F. Yao, X.H. Xu, H. Wang, J.T. Zhou, X.N. Yang, Y. Zhang, S.X. Shang, B.B. Huang, Photocatalytic property of perovskite bismuth titanate, Appl. Catal. B Environ. 52 (2004) 109–116. https://doi.org/10.1016/j.apcatb.2004.04.002.
[45]W. Feng Yao, H. Wang, X. Hong Xu, X. Feng Cheng, J. Huang, S. Xia Shang, X. Na Yang, M. Wang, Photocatalytic property of bismuth titanate Bi12TiO20 crystals, Appl. Catal. Gen. 243 (2003) 185–190. https://doi.org/10.1016/S0926-860X(02)00564-1.
[46]L. Wang, W. Ma, Y. Fang, Y. Zhang, M. Jia, R. Li, Y. Huang, Bi4Ti3O12 Synthesized by High Temperature Solid Phase Method and it's Visible Catalytic Activity, Procedia Environ. Sci. 18 (2013) 547–558. https://doi.org/10.1016/j.proenv.2013.04.074.
[47]M. Valant, D. Suvorov, Processing and Dielectric Properties of Sillenite Compounds Bi12MO20−δ (M = Si, Ge, Ti, Pb, Mn, B1/2P1/2), J. Am. Ceram. Soc. 84 (2001) 2900–2904. https://doi.org/10.1111/j.1151-2916.2001.tb01112.x.

[48]T. Kikuchi, A. Watanabe, K. Uchida, A family of mixed-layer type bismuth compounds, Mater. Res. Bull. 12 (1977) 299–304. https://doi.org/10.1016/0025-5408(77)90148-9.
[49]W. Wei, Y. Dai, B. Huang, First-Principles Characterization of Bi-based Photocatalysts: Bi12TiO20, Bi2Ti2O7, and Bi4Ti3O12, J. Phys. Chem. C. 113 (2009) 5658–5663. https://doi.org/10.1021/jp810344e.
[50]G.A. Kallawar, D.P. Barai, B.A. Bhanvase, Bismuth titanate based photocatalysts for degradation of persistent organic compounds in wastewater: A comprehensive review on synthesis methods, performance as photocatalyst and challenges, J. Clean. Prod. 318 (2021) 128563. https://doi.org/10.1016/j.jclepro.2021.128563.
[51]M. Grao, J. Redfern, P.J. Kelly, M. Ratova, Magnetron co-sputtered Bi12TiO20/Bi4Ti3O12 composite – An efficient photocatalytic material with photoinduced oxygen vacancies for water treatment application, Appl. Surf. Sci. 552 (2021) 149486. https://doi.org/10.1016/j.apsusc.2021.149486.
[52]T.S. Rajaraman, S.P. Parikh, V.G. Gandhi, Black TiO2: A review of its properties and conflicting trends, Chem. Eng. J. 389 (2020) 123918. https://doi.org/10.1016/j.cej.2019.123918.
[53]X. Chen, L. Liu, P.Y. Yu, S.S. Mao, Increasing solar absorption for photocatalysis with black hydrogenated titanium dioxide nanocrystals, Science. 331 (2011) 746–750. https://doi.org/10.1126/science.1200448.
[54]L. Ye, L. Zan, L. Tian, T. Peng, J. Zhang, The {001} facets-dependent high photoactivity of BiOCl nanosheets, Chem. Commun. 47 (2011) 6951–6953. https://doi.org/10.1039/C1CC11015B.
[55]M. Grao, M. Ratova, P. Kelly, Design and optimisation of a low-cost titanium dioxide-coated stainless steel mesh photocatalytic water treatment reactor, J. Clean. Prod. (2021) 126641. https://doi.org/10.1016/j.jclepro.2021.126641.
[56]Synthesis of Best-Seller Drugs, Elsevier, 2016. https://doi.org/10.1016/C2012-0-07004-4.
[57]G.J. Anderson, Quinolone Antimicrobial Agents, 3rd Edition, Emerg. Infect. Dis. 10 (2004) 1177. https://doi.org/10.3201/eid1006.040025.
[58]Y.-H. Chiu, T.-F.M. Chang, C.-Y. Chen, M. Sone, Y.-J. Hsu, Mechanistic Insights into Photodegradation of Organic Dyes Using Heterostructure Photocatalysts, Catalysts. 9 (2019) 430. https://doi.org/10.3390/catal9050430.
[59]J. Tauc, Optical properties and electronic structure of amorphous Ge and Si, Mater. Res. Bull. 3 (1968) 37–46. https://doi.org/10.1016/0025-5408(68)90023-8.
[60]Q. Liu, Y. Guo, Z. Chen, Z. Zhang, X. Fang, Constructing a novel ternary Fe(III)/graphene/g-C3N4 composite photocatalyst with enhanced visible-light driven photocatalytic activity via interfacial charge transfer effect, Appl. Catal. B Environ. 183 (2016) 231–241. https://doi.org/10.1016/j.apcatb.2015.10.054.
[61]J. Liang, Y. Wei, Y. Yao, X. Zheng, J. Shen, G. He, H. Chen, Constructing high-efficiency photocatalyst for degrading ciprofloxacin: Three-dimensional visible light driven graphene based NiAlFe LDH, J. Colloid Interface Sci. 540 (2019) 237–246. https://doi.org/10.1016/j.jcis.2019.01.011.
[62]R. Gupta, B. Boruah, J.M. Modak, G. Madras, Kinetic study of Z-scheme C3N4/CuWO4 photocatalyst towards solar light inactivation of mixed populated bacteria, J. Photochem. Photobiol. Chem. 372 (2019) 108–121. https://doi.org/10.1016/j.jphotochem.2018.08.035.
[63]K. Ding, W. Wang, D. Yu, W. Wang, P. Gao, B. Liu, Facile formation of flexible Ag/AgCl/polydopamine/cotton fabric composite photocatalysts as an efficient visible-light photocatalysts, Appl. Surf. Sci. 454 (2018) 101–111. https://doi.org/10.1016/j.apsusc.2018.05.154.
[64]W. Deng, H. Zhao, F. Pan, X. Feng, B. Jung, A. Abdel-Wahab, B. Batchelor, Y. Li, Visible-Light-Driven Photocatalytic Degradation of Organic Water Pollutants Promoted by Sulfite

Addition, Environ. Sci. Technol. 51 (2017) 13372–13379. https://doi.org/10.1021/acs.est.7b04206.
[65]W. Guo, Y. Yang, Y. Guo, Y. Jia, H. Liu, Y. Guo, Self-assembled hierarchical Bi12TiO20–graphene nanoarchitectures with excellent simulated sunlight photocatalytic activity, Phys. Chem. Chem. Phys. 16 (2014) 2705–2714. https://doi.org/10.1039/C3CP53070A.
[66]M. Arya, M. Kaur, A. Kaur, S. Singh, P. Devi, S.K. Kansal, Hydrothermal synthesis of rGO-Bi2WO6 heterostructure for the photocatalytic degradation of levofloxacin, Opt. Mater. 107 (2020) 110126. https://doi.org/10.1016/j.optmat.2020.110126.
[67]X. Zhong, K.-X. Zhang, D. Wu, X.-Y. Ye, W. Huang, B.-X. Zhou, Enhanced photocatalytic degradation of levofloxacin by Fe-doped BiOCl nanosheets under LED light irradiation, Chem. Eng. J. 383 (2020) 123148. https://doi.org/10.1016/j.cej.2019.123148.
[68]B. Gulen, P. Demircivi, E.B. Simsek, UV-A light irradiated photocatalytic performance of hydrothermally obtained W doped BaZrO3 catalyst against the degradation of levofloxacin and tetracycline antibiotic, J. Photochem. Photobiol. Chem. 404 (2021) 112869. https://doi.org/10.1016/j.jphotochem.2020.112869.
[69]J. Nie, X. Yu, Z. Liu, Y. Wei, J. Zhang, N. Zhao, Z. Yu, B. Yao, Boosting principles for the photocatalytic performance of Cr-doped Cu2O crystallites and mechanisms of photocatalytic oxidation for levofloxacin, Appl. Surf. Sci. 576 (2022) 151842. https://doi.org/10.1016/j.apsusc.2021.151842.
[70]K.P. Sundar, S. Kanmani, Progression of Photocatalytic reactors and it's comparison: A Review, Chem. Eng. Res. Des. 154 (2020) 135–150. https://doi.org/10.1016/j.cherd.2019.11.035.